Metallurgical Aspects and Wear Performance of Al/(Fe−Cu)$_p$ Hybrid Composite Produced Using Friction Stir Processing

Mehran Karimi Estahbanati[1] · Mojtaba Movahedi[1]

Abstract

Al1050/(Fe–Cu) hybrid surface composite was produced using friction stir processing (FSP). The effects of the weight fraction ratio of Fe and Cu powders in the composite and the process pass number (3 and 5 passes) were investigated on the wear performance and microstructural features of the composite. The results showed that Al–Fe and Al–Cu binary and Al–Fe–Cu ternary intermetallic compounds were in-situ formed at the interface of the Fe–Cu powders and Al matrix. Non-uniform distribution of the micron-sized and sub-micron particles in the stir zone had a main role in the formation of the bi-modal grain structure in the composite. The average friction coefficient of the composites decreased (up to ∼40%) and the wear resistance of the composites improved (up to ∼85%) compared to the specimen processed without the reinforcing particles. The composites with the equal weight fraction of Fe and Cu particles and the composites processed at 5 FSP passes showed superior wear performance. The wear mechanism was changed from the adhesive wear in the 75Cu–25Fe-3 passes and 75Fe–25Cu-3 passes composites to the delamination wear in the 50Fe–50Cu-5 passes composite. The mentioned results were discussed in the light of the metallurgical aspects of the produced composites, i.e. uniformity of the aluminum matrix grain structure and distribution of the reinforcing particles as well as the amount of the intermetallic compounds formed in the composites.

Keywords Friction stir processing · Aluminum hybrid composite · Microstructure · Intermetallic compound · Hardness · Wear resistance

1 Introduction

Aluminum alloys have attracted much attention in aerospace, marine equipment, and automobile industries due to their high specific strength, high thermal conductivity and good corrosion resistance. However, the low wear resistance of the aluminum and its alloys limits their application. In order to overcome this issue, aluminum matrix composites (AMCs) with excellent mechanical and tribological properties have been used in various industries [1]. The employed methods to produce AMCs can be categorized into solid and liquid states processes. Generally, unfavorable physical and mechanical properties may be observed in the liquid state processes because of the poor wettability and interfacial

bonding between the reinforcements and aluminum matrix along with the solidification cracks. Reduction of the process temperature below the melting point of the matrix in the solid state processes can lessen the mentioned problems associated with the liquid state processes [2, 3]. Xie et al. [4] presented a new solid state method for achieving an excellent balance between high strength and ductility namely as deformation-driven metallurgy (DDM) to overcome several disadvantages of liquid state processes. Friction stir processing (FSP) is one of the solid state processes used for production of the metal matrix composites that was first devised based on the concept of the friction stir welding (FSW) [5]. In FSP, a non-consumable rotating tool including a shoulder and pin is plunged in the base metals and traverses a specified path on the workpiece for the microstructural modification as well as the dispersion of the reinforcing particles in the stir zone (SZ). Heat generated by friction between the FSP tool and the surrounding material along with the severe plastic deformation in the SZ softens the material around the tool and facilitates the material flow [5]. Simultaneous presence

✉ Mojtaba Movahedi
  m_movahedi@sharif.edu

1   Department of Materials Science and Engineering, Sharif
    University of Technology, Azadi Ave., PO Box 11365-9466,
    Tehran, Iran

of the severe plastic deformation and high temperature in the SZ results in the occurrence of the dynamic recrystallization (DRX) leading to the grain refinement [6, 7].

Ceramic and metallic powders are usually employed to produce AMCs. Ceramic particles are generally used to enhance the hardness of the composites directly [5, 8, 9]. On the other hand, metallic powders are used as the reinforcement to react with the matrix and form intermetallic compounds (IMCs) during the process. This kind of composite called in-situ composite benefits from various advantages such as more homogeneous microstructure as well as the stronger interfacial bonding between the reinforcing particles and the matrix improving the hardness and wear performance of the composites [10]. Meng et al. [11] fabricated a gradient coating on the AA6082-T6 substrate via in-situ arc surface nitriding with subsequent friction stir processing. They reported that the wear resistance remarkably improved. Huang et al. [12] examined the microstructural and mechanical properties of the Al matrix composite in which pure copper powder was used as the reinforcement. They observed that increasing the FSP pass number can enhance the in-situ reaction of Al matrix/Cu particle and formation of Al_2Cu intermetallics. They also reported that, by compositing, the wear resistance of the samples improved up to ~35%, compared to the as-received Al matrix. Abhishek et al. [13] fabricated the aluminum matrix composites reinforced with Ti_6Al_4V particles and found out that Ti–Al intermetallics were formed during the FSP. Moreover, they observed that the subsurface cracks formed during the wear test, were away from the reinforcements (Ti_6Al_4V and TiAl). Due to the presence of both Ti_6Al_4V and TiAl particles, the wear resistance of the composite improved ~46% compared to the unreinforced specimen.

Hybrid AMCs are fabricated by two or more kinds of the reinforcing particles in order to profit the combined advantages of the reinforcements along with the reduction in the agglomeration of the reinforcing particles [14, 15]. According to the best knowledge of the authors, no investigation has been made so far on the aluminum matrix composite reinforced with the hybrid reinforcements of the Fe and Cu particles. Using of the Fe and Cu particles as the reinforcements in FSP can increase the mechanical properties of the composites by the particles themselves and the formation of intermetallics during the FSP [16–18]. The simultaneous presence of the Fe and Cu powders in the matrix can diminish the possibility of the intimate contact between the similar powders and consequently, the agglomeration of

the particles can be decreased. Therefore, the aim of this research was the producing of Al/(Fe–Cu)$_p$ hybrid composite by FSP and studying the effects of the powder weight ratio of Fe–Cu reinforcements and FSP pass number on the metallurgical features and mechanical properties of the composites. The focus is on the wear behavior.

2 Experimental Procedure

Al-1050 sheets with the dimensions of 150 mm × 70 mm × 4 mm were used as the base metal. The chemical composition and mechanical properties of the Al-1050 base metal are reported in Table 1. Fe and Cu powders with purity of 99.5% and the average sizes of ~ 10 and 14–25 μm, respectively, were used as the reinforcing particles.

Since using different weight ratios of the Cu and the Fe powders can affect formation of the diverse IMCs and the agglomeration degree of the particles, three weight ratios of 75Fe–25Cu, 50Fe–50Cu and 75Cu–25Fe were used for making the composites. A tubular mixing machine was used to mix the hybrid powders for 30 min. In order to insert the reinforcing powders inside the aluminum matrix, a groove with the cross-section dimensions of 2 mm width and 3 mm depth was cut at the center and along the rolling direction of the sheets. After inserting the powders inside the groove, a rotating pin free tool was used to close the groove and prevent the powders to spread out during the FSP. Then, the FSP tool made from H13 tool steel with the hardness of 52–54 RC including the pin and shoulder was used for 3 and 5 passes of the FSP. The schematic and the dimensions of the FSP tool are shown in Fig. 1a.

Rotational speed, traveling speed and tilt angle of the FSP tool were constant at 1400, 10 cm/min and 3°, respectively. Compared to the retreating side, the advancing side of the SZ experiences more temperature and stirring action [15, 16]. Therefore, in order to acquire more homogeneous properties in the composite, the rotation orientation of the FSP tool was reversed in each pass. In other words, the advancing side of each pass was the retreating side of the previous pass. Moreover, three samples, as the reference, were FSPed at the same conditions without using particles and using just one kind of particle, i.e. Fe or Cu, in five passes to evaluate the effect of the added particles and hybrid particles on the mechanical properties, compared to the non-composite samples. Given the dimension and geometry of the stir zone

Table 1 Chemical composition (wt%) and mechanical properties of the as-received Al-1050 base sheet

Chemical composition (wt%)				Mechanical properties		
Al	Si	Fe	Zn	UTS (MPa)	Hardness (Hv)	Strain to fracture (%)
Bal	0.06	0.4	0.02	76	31	53

Fig. 1 The schematic and dimensions of **a** the FSP tool with pin and **b** the FSPed specimen showing the process accomplishment and sample preparation for microstructure and wear properties examinations (dimensions are in mm)
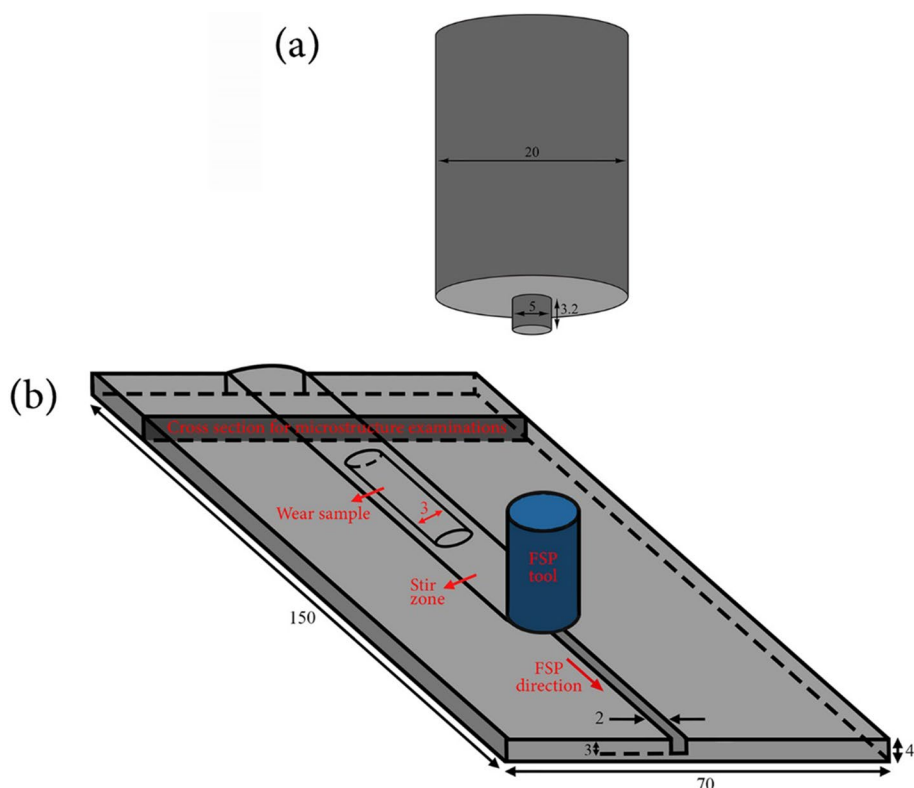
as well as the weight of the reinforcing particles inserted inside the groove, composites with ~ 3 wt% of the reinforcing particles were produced.

For microstructural studies, the cross-sections of the FSPed samples were prepared by the standard metallographic procedures and then were electro-etched in the solution with composition of 100 ml HBF$_4$ (2.5%) + 10 ml HF in the voltage of 20 V for 300 s. Optical microscope (OM) equipped with the polarized light was used to observe the grain structure of the composite. Field emission scanning electron microscopy (FESEM) and energy dispersive X-ray spectroscopy (EDS) were employed for examination of the powder distribution and the worn-out surfaces of the composites. Also, X-ray diffraction (XRD) analysis (with Cu-Kα ray) was used to identify the formed phases. Moreover, the IMCs formed at the interface of the Al matrix/Fe particle and Al matrix/Cu particle after the FSP were characterized by FESEM equipped with EDS. In order to investigate the mechanical properties of the FSPed composites, Vickers microhardness test along with the wear test were performed. The microhardness test was carried out on the cross-section of the specimens at the centerline of the SZ by a load of 200 g applied for 15 s.

The wear behavior of the specimens was evaluated by the pin-on-disk test carried out based on ASTM G99-04 standard. For this test, the composites were cut in the shape of a pin and a SPK steel disk (Cr = 12 wt%, C = 1.2080 wt%,

Fe = bulk) with the hardness of 700 HV was used as the counterpart. The diameter and height of the SPK disk were 50 mm and 9 mm, respectively. The pins were cut in the cylindrical shape from the stir zone with the diameter of 3 mm and height of 30 mm (Fig. 1b). After polishing and cleaning by acetone, pins were weighed with the accuracy of 0.0001 g. The wear test was performed in the sliding distance of 1000 m with 250 m intervals under the normal atmosphere in the ambient temperature and without using any lubricant. The nominal load and sliding velocity of the pin were 30 N and 0.23 ms^{-1}, respectively. At each interval, the samples were weighed again and the weight loss was recorded. The coefficient of the friction was automatically determined by a tribometer.

3 Results and Discussion

3.1 Microstructure of Composite

3.1.1 Distribution of Reinforcing Particles

Figure 2 shows the FESEM images from distribution of the reinforcing particles in the SZ. As can be seen, the added particles in 100Cu and 100Fe composites (Fig. 2a, b, respectively) were highly agglomerated even after 5 passes. This observation was expected since when just one kind of the
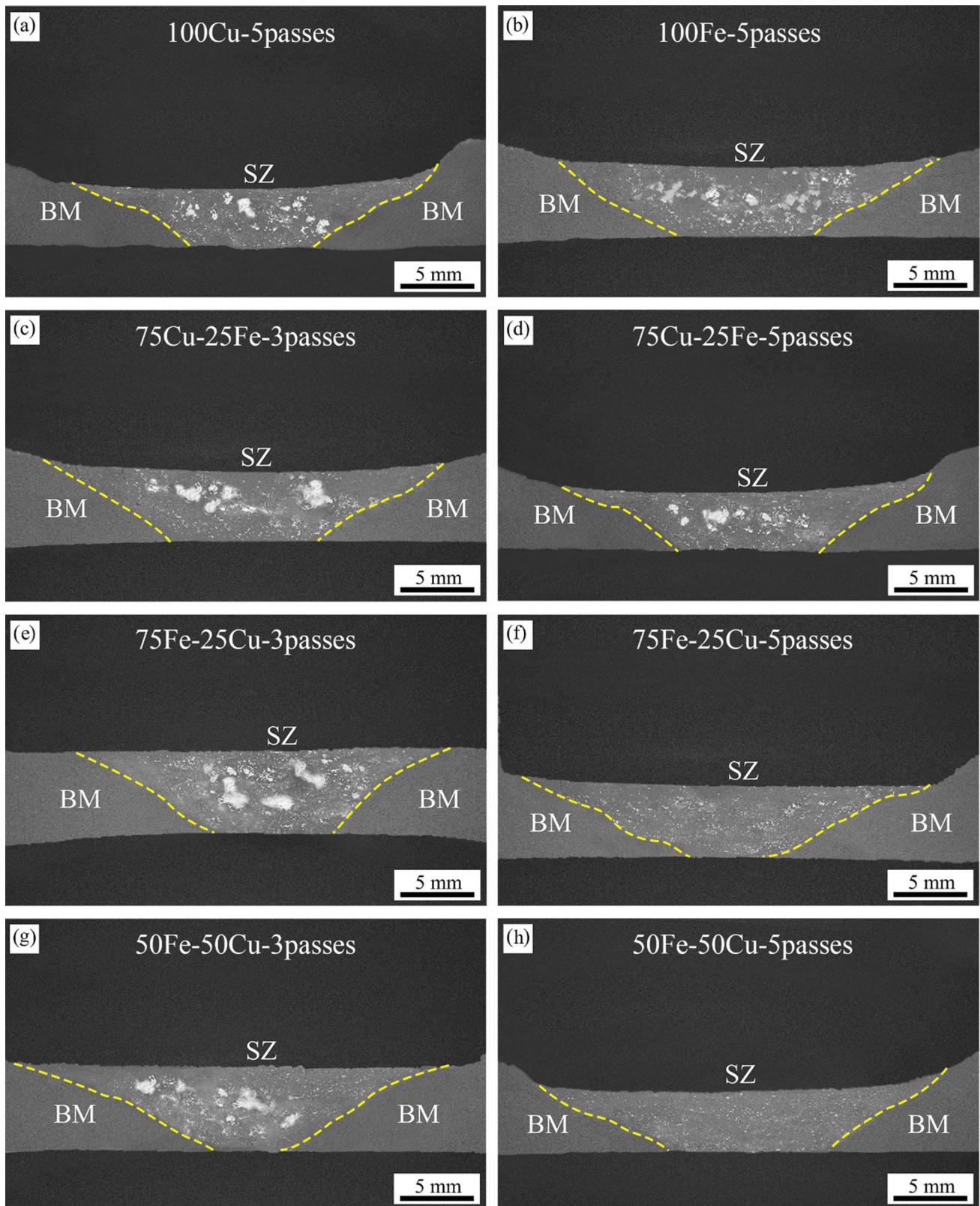
Fig. 2 FESEM images from the stir zone of the composites

particle is added to the aluminum matrix, the possibility of the intimate contact between the similar particles increases and thus, agglomeration of the particles is facilitated.

Another observation is that the distribution of the particles became more homogeneous and the size of the clustered particles was reduced by increasing the FSP pass number from 3 to 5. In other words, the more was the FSP pass number, the more uniform was the distribution of the Fe and Cu particles in the Al matrix for all combinations of the Fe and Cu powders. This is an expected result because of more rotating action of the tool and material flow as well as the deformation in the SZ at the higher FSP number during the process.

Fe/Cu powder weight ratio significantly affected the distribution of the reinforcing particles in the SZ. In a constant FSP pass number, the best distribution of the reinforcements was related to the composites with the powder weight ratio of 50Fe–50Cu (Fig. 2). Moreover, in the composites with the powder weight ratio of 75Cu–25Fe, agglomeration of the particles was so intensive even after 5 passes of FSP (Fig. 2c and d). The reason can be attributed to the bigger size of the Cu particles compared to the Fe particles used in this work that prevented the particles to flow easily in the stir zone during the FSP.
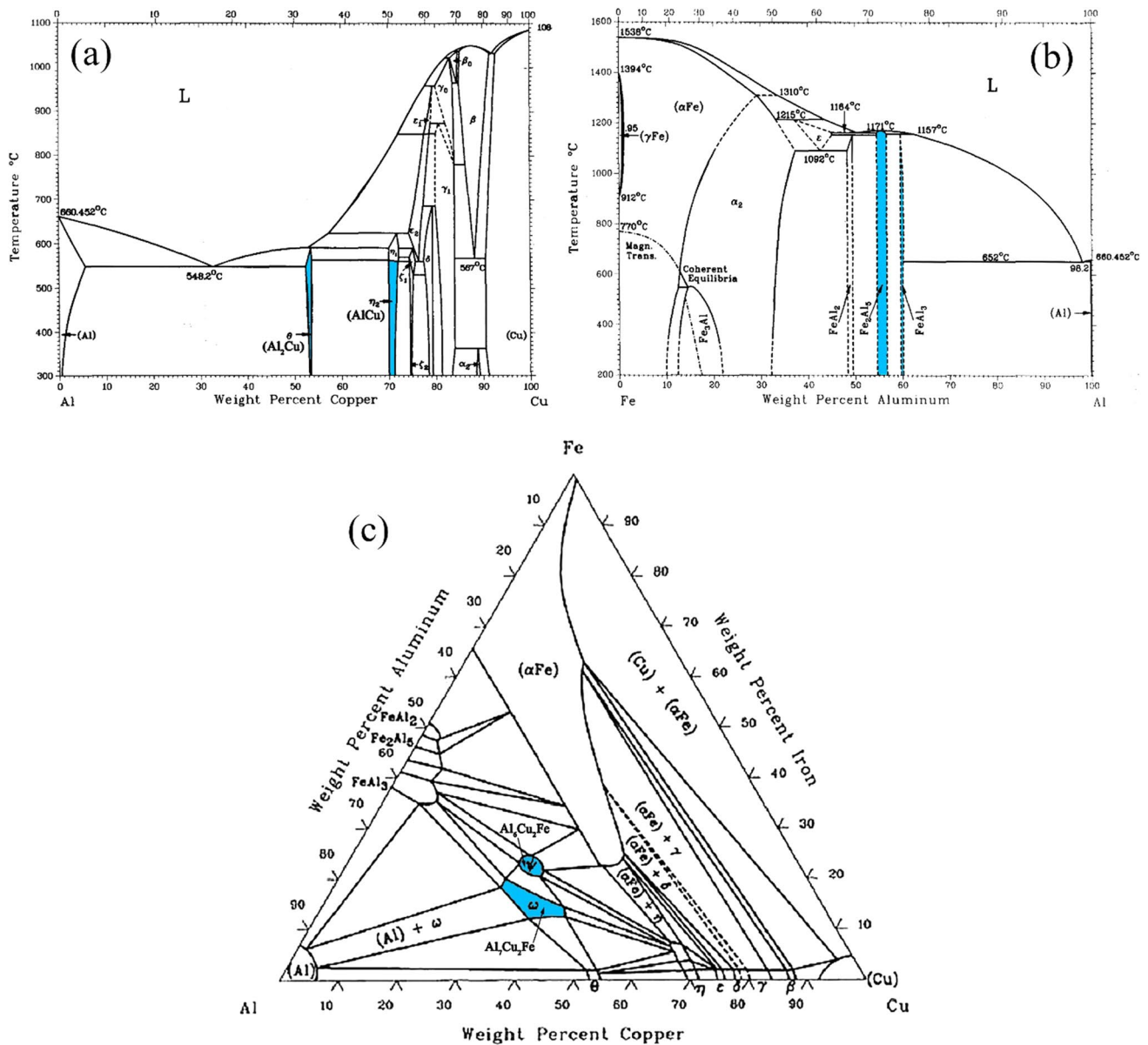

Fig. 3 Phase diagrams of **a** Al–Cu, **b** Al–Fe binary systems [19] and **c** 600 °C isothermal section of the Al–Fe–Cu ternary system [20]
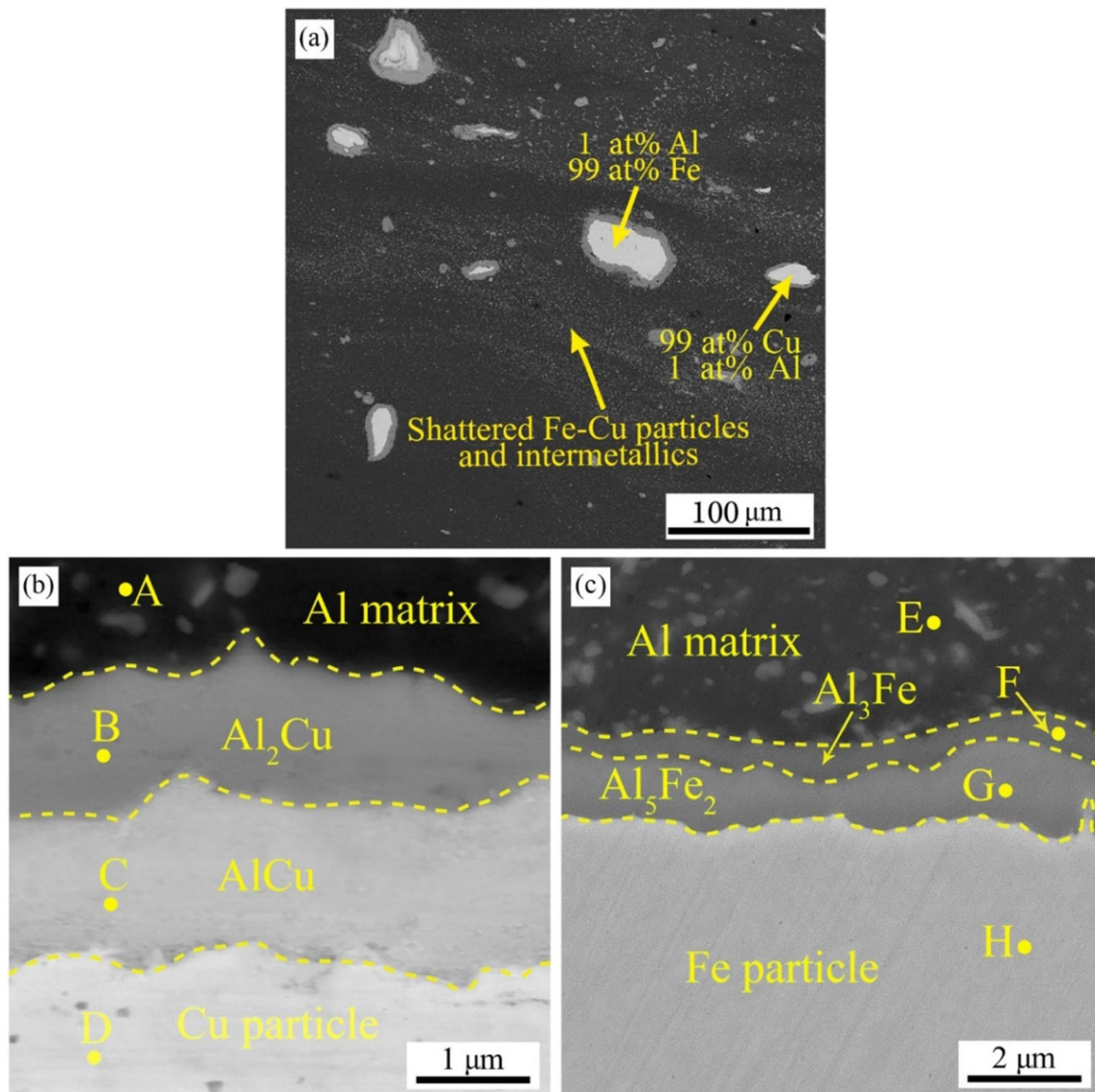
Fig. 4 FESEM images from **a** the stirred zone and **b** and **c** the IMCs at the interface of Cu and Fe particles, respectively, with the Al matrix in the 50Fe–50Cu-3 passes composite

Table 2 EDS analysis results of the locations shown in Fig. 4

Location in Fig. 4	Measured composition (at%)			Nominal composition of IMCs	Identified substance
	Cu	Fe	Al		
A	2	0	98	–	Al matrix
B	33	0	67	Al$_2$Cu: 67–68 at% Al, 32–33 at% Cu	Al$_2$Cu
C	52	0	48	AlCu: 49–50.5 at% Al, 49.5–51 at% Cu	AlCu
D	99	0	1	–	Cu particle
E	0	4	96	–	Al matrix
F	0	23	77	Al$_3$Fe: 74.5–76.5 at% Al, 23.5–25.5 at% Fe	Al$_3$Fe
G	0	25	75	Al$_5$Fe$_2$: 70–73 at% Al, 27–30 at% Fe	Al$_5$Fe$_2$
H	0	100	0	–	Fe particle

3.1.2 Intermetallic Compounds

Given the high temperature experienced in the SZ during the FSP, in-situ intermetallic compounds can be formed at the interface of the metallic reinforcing particles and the Al matrix. Binary IMCs of Al_2Cu, $AlCu$, Al_9Cu_{11}, $AlCu_2$, Al_4Cu_9, $AlCu_4$ and binary IMCs of Al_3Fe, Al_5Fe_2, Al_2Fe, $AlFe$, $AlFe_3$ are observed in the Al–Cu (Fig. 3a) and Al–Fe (Fig. 3b) phase diagrams, respectively. Moreover, ternary IMCs of Al_6Cu_2Fe and Al_7Cu_2Fe can be formed according to the Al–Fe–Cu (Fig. 3c) phase diagram at 600 °C isothermal section.

Figure 4 shows the FESEM images from the SZ of the 50Fe–50Cu-3 passes composite. As it is clear in Fig. 4a, although the shattered Fe and Cu particles and IMCs were dispersed in the SZ, some agglomerated Fe and Cu particles were also evident. It is obvious that a reaction layer has been in-situ formed at the interfaces of the Fe and Cu powders and Al matrix. According to Fig. 4b and c, at both interfaces, two intermetallic layers with different contrasts are formed. In order to determine the chemical composition of the IMCs, EDS analysis was conducted at the locations shown in Fig. 4b and c and the results are reported in Table 2.

The result of the EDS analysis at the specified areas in Fig. 4b confirmed that Al_2Cu and $AlCu$ were formed adjacent to the Al matrix and Cu particle, respectively. On the other hand, according to Fig. 4c and the EDS analysis results, Al_3Fe and Al_5Fe_2 were formed at the interface of the Al matrix and Fe particle. Some previous studies were investigated the formation of the IMCs at the Al–Fe and Al–Cu interfaces and reported that Al_3Fe (next to the Al) and Al_5Fe_2 (next to the the Fe) were formed at the Al–Fe interface [16, 21]. Moreover, $AlCu$ (adjacent to the Cu) and Al_2Cu (adjacent to the Al) were stated to be formed at the Al–Cu interface [17, 18].

For more investigations, the XRD analysis was performed on the SZ of the 50Fe–50Cu-5 passes composite. As can be seen in Fig. 5, some peaks of Al_5Fe_2, Al_2Cu, and Al_7Cu_2Fe IMCs are evident in the XRD pattern confirming that these phases were formed at the SZ. The absence of the peaks of the other IMCs in the XRD pattern can be due to their low quantity in the SZ.

The EDS point analysis and the thickness of the IMCs formed at the interface of the Cu particles in the 75Cu–25Fe-3 passes, 75Cu–25Fe-5 passes, and 50Fe–50Cu-5 passes composites are shown in Fig. 6a–d. Additionally, the EDS line analysis was conducted along the yellow line shown in Fig. 6c. As can be seen, intermetallic compounds and the type of reinforcing particles in the composites can be distinguished using EDS point and line analyses. It can be concluded that the FSP pass number and the weight ratio of the powders do not have any tangible effect on the thickness of the IMCs. It can be due to the continuously forming and shattering of the IMCs during the FSP.

3.1.3 Grain Structure

Figure 7a shows the grain structure of the base metal. As can be seen, the as-received base metal had an elongated grain structure. In addition, the SZ of the sample processed by 5 passes of FSP without reinforcing powders shown in Fig. 7b included equiaxed grains with the average grain size of ~21 μm due to the recrystallization and grain growth which occurs during FSP as a result of the severe plastic deformation accompanied by the high temperature in the SZ [6, 7].

The grain structures of the composites are also indicated in Fig. 7. It should be noted that the dark areas in the microstructures are agglomerates of the reinforcing particles corroded severely during the etching process. It is obvious that the grain structures of the 100Cu-5 passes and 100Fe-5 passes composites were noticeably non-homogeneous as a

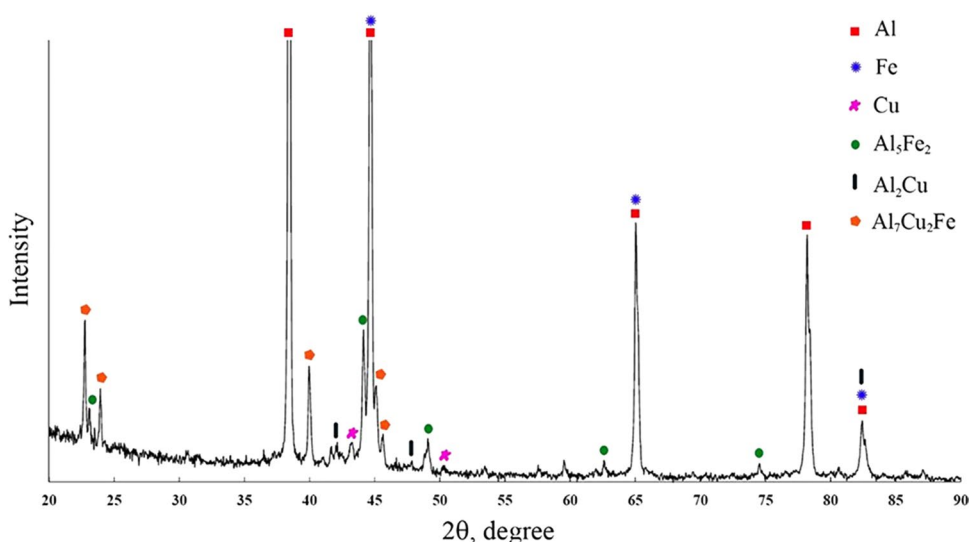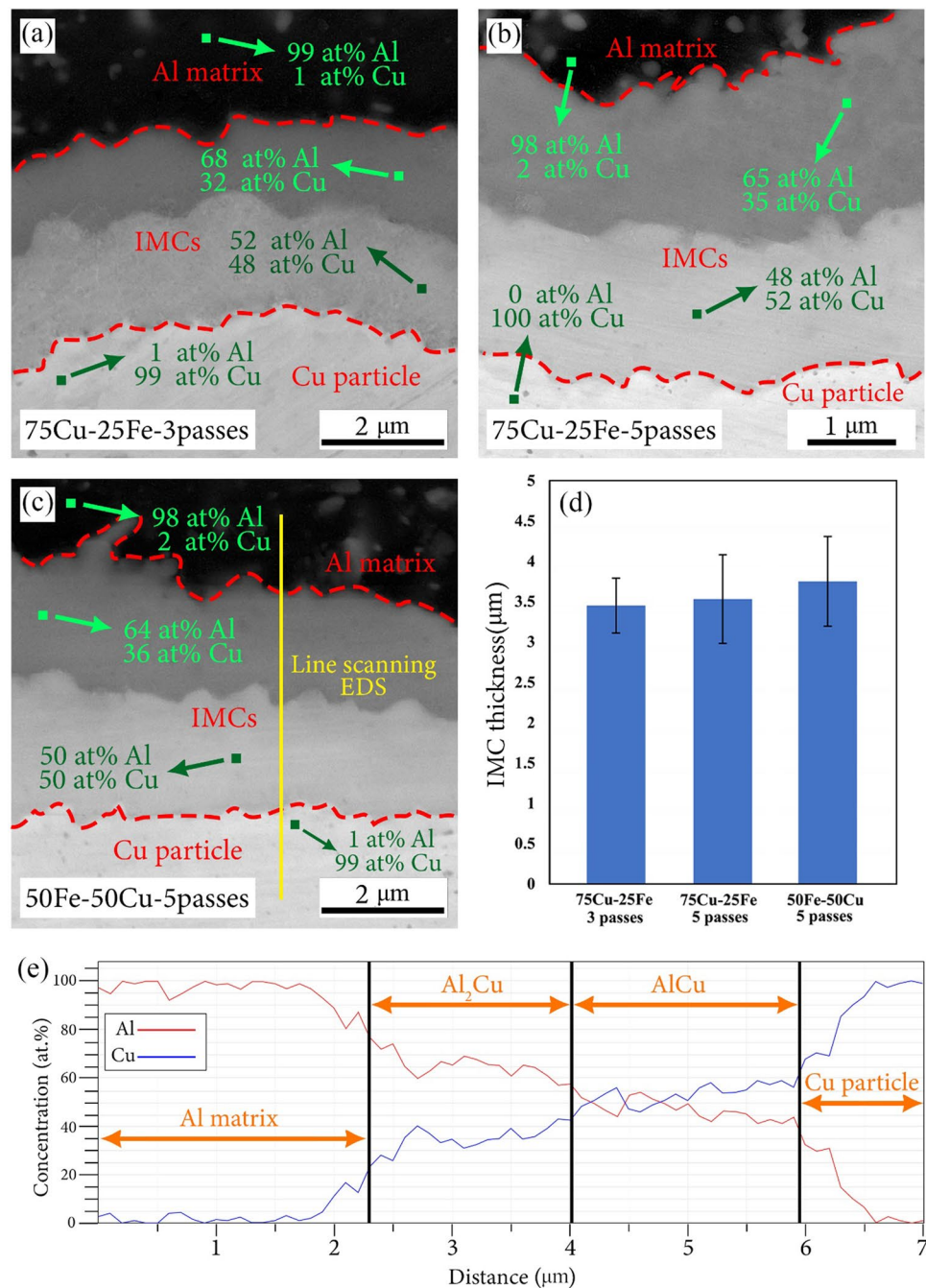**Fig. 5** XRD pattern from the stir zone of the 50Fe–50Cu-5 passes composite

Fig. 6 FESEM images showing the thickness of the IMCs formed at the Cu particle/Al matrix interface in the **a** 75Cu–25Fe-3 passes, **b** 75Cu–25Fe-5 passes and **c** 50Fe–50Cu-5 passes composites. **d** Measured thickness of the IMCs and **e** the EDS line analysis conducted along the yellow line shown in **c**

result of the non-uniform distribution of the reinforcing particles as described in Sect. 3.1.1 (Fig. 7c, d). Increase in the FSP pass number led to the more homogeneous grain structure due to more homogeneous particle distribution inside the SZ. Moreover, at a certain pass number, the composite containing the powder weight ratio of 75Cu–25Fe (with the most agglomerated particles) had the most non-homogeneous grain structure compared to the other composites.

For more evaluation of the non-homogeneity in the grain structure, the optical microscope images from the same region in the SZ of the 75Fe–25Cu-3 passes composite,

before and after etching, are shown in Fig. 8a and b, respectively. While the image before etching clearly shows the distribution of the reinforcing particles, the etched microstructure displays the grain structure of the composite. Figure 8b presents two distinct grain structure regimes: fine grain structure and coarse grain structure. Given the optical microscope images before and after etching, the regions with fine grains are rich of the reinforcing particles. However, the regions poor of the reinforcing particles consist of the coarse grains. The average grain size of the coarse and the fine grain regions are ~ 17 and ~ 1 μm, respectively. Figure 8c

displays the boundary between the coarse and fine grains at higher magnification. The second phase particles inside the SZ, depending on their size, may decrease the grain size during the dynamic recrystallization process via two different mechanisms:

- *Particle stimulated nucleation (PSN)* The micron-sized particles i.e. Fe and Cu particles, due to different strain behavior compared to the aluminum matrix, the presence of the stress concentration and accumulation of dislocations around them are preferred sites for the nucleation of new grains. This mechanism is known as the PSN [22].
- *Pinning effect of the grain boundaries* The FESEM image from the fine grain regions is presented in Fig. 8d. As can be seen, there were sub-micron particles in the aluminum matrix. These particles are fragmented Fe and Cu reinforcements as well as the IMCs formed in-situ during FSP and shattered due to brittle nature and stirring action of the FSP tool. Sub-micron particles can act as a barrier to the movement of the grain boundaries of the newly recrystallized grains during the dynamic recrystallization and prevent the grains to grow (i.e. pinning effect of the sub-micron particles) [23, 24].

Therefore, the non-homogeneous distribution of the micron-sized and sub-micron particles in the SZ played a main role in the formation of the bi-modal grain structure in the composite.

3.2 Mechanical Properties

3.2.1 Microhardness

Microhardness profile and the average microhardness of the SZ and base metal in the samples are presented in Fig. 9a and b, respectively. As can be seen, the microhardness of the stir zone for all composites increased compared to the base metal and the sample processed without powder. The main causes can be summarized as follows [16, 25, 26]:

- grain refinement of the Al matrix due to occurrence of the dynamic recrystallization and presence of the second phase particles as discussed in Sect. 3.1.3,
- higher microhardness of the Fe and Cu powders compared to aluminum matrix,
- in-situ formation of the IMCs with high microhardness between the Fe/Cu particles and the Al matrix and the subsequent dispersion of the shattered IMCs inside the Al matrix due to the stirring action of the FSP tool,
- pinning of the dislocations because of the presence of the sub-micron particles (Orowan mechanism),

- high density of the dislocations around the reinforcing particles caused by the different coefficients of the thermal expansion (CTE) of the reinforcing particles and the Al matrix.

Referring to Fig. 9a, the microhardness profile of the SZ in the 100Cu-5 passes and 100Fe-5 passes composites and the composites produced at 3 passes showed further fluctuation compared to the hybrid composites processed at 5 passes. As explained in Sect. 3.1.1, the mentioned composites had a non-uniform distribution of the reinforcing particles in comparison to the hybrid composites processed at 5 passes. Therefore, during the hardness test, the indenter intermittently touched the regions rich and poor of the reinforcing particles.

According to Fig. 9b, with enhancement of the FSP pass number from 3 to 5 passes and by using the hybrid reinforcements, the average hardness of the composites increased. This was due to the more uniform distribution of the reinforcing particles at the hybrid composites and after 5 passes compared to 3 passes. In fact, the more uniform is the distribution of the Fe and Cu powders, the more is the surface contact between these powders and the aluminum matrix. Additionally, more FSP pass number provides more time for inter-diffusion of Al and Fe/Cu atoms between the reinforcing particles and the matrix. Both of the mentioned phenomena lead to the formation of more IMCs in the composites. In the composites made by just one kind of particle, the lower contact surface between the agglomerated particles and the aluminum matrix due to unfavorable dispersion of the reinforcements led to an inferior inter-diffusion of the atoms. From this point of view, the 50Fe–50Cu-5 passes composite had the maximum hardness (~ 3 times higher compared to the sample processed at 5 passes without powder) due to the most uniform distribution of the reinforcing powders as mentioned in Sect. 3.1.1.

3.2.2 Wear

3.2.2.1 Friction Coefficient Figure 10 shows the friction coefficient of the composites and the specimen processed without reinforcing particles obtained from the wear test. Because of the unfavorable microstructural and mechanical properties, the wear behavior of the composites made by just one kind of particle was not evaluated. Fluctuations in the friction coefficient of the specimens were evident. In fact, because of the heat generation and high temperature during the wear process, surfaces of the pin and disk are exposed to the oxidation. Existence of an oxide film on the surfaces of the pin and disk decreases the friction coefficient. In effect of the load applied to the pin during the wear test, the oxide film is destroyed. Since the virgin metals have more adhesion compared to the oxide film and metal, the

friction coefficient increases again [27]. Squeezing out of the reinforcing particles between the surfaces of the pin and the counterpart during the wear may also be effective on these fluctuations [28].

For investigating the influence of the Fe/Cu powder weight ratio and the FSP pass number on the wear behavior of the composites, the mean friction coefficients of the samples are reported in Table 3.

The highest friction coefficient was 0.74 for the sample processed in 5 passes without reinforcing powders. By compositing, the mean friction coefficient decreased up to ~40%. The minimum friction coefficient belonged to the 50Fe–50Cu composite processed at 5 passes. Regarding to the 3.1 sections, using the powder weight ratio of 50Fe–50Cu and enhancement of the FSP pass number from 3 to 5 resulted in the most uniform grain structure and distribution of the reinforcing particles. Existence of the hard and homogeneously dispersed particles in the composite matrix led to protection of the Al matrix during the wear test and reduction of the friction coefficient [26].

3.2.2.2 Weight Loss The weight loss of the specimens as a function of the sliding distance is shown in Fig. 11. It is clear that the wear resistance of the composites improved considerably compared to the specimen processed without the reinforcing particles. This result was expected due to the higher hardness of the composites caused by the finer grain structure and presence of the Fe/Cu particles and the in-situ formed intermetallic compounds [26, 29–34].

Figure 11 shows that the wear resistance of the composites produced in 5 passes was considerably more than that in 3 passes. This was also true for the 50Fe–50Cu composite in comparison to the other composites. The origin of this observation is the improved distribution of the reinforcing particles inside the Al matrix resulting in the formation of the fine and homogeneous grain structure as well as the higher amount of the IMCs and the related hardness of the composites (as discussed before). Furthermore, Fig. 9a indicates that hardness profiles for the 50Fe–50Cu composites and for the composites processed at 5 passes are almost consistent with no abrupt changes in different regions of the SZ. The consistent distribution of the hardness as a result of the homogeneous distribution of the particles in the composites may be effective on the higher wear resistance. This finding is in agreement with the results of the research carried out by Paidar et al. [26] as dispersion of the powders and hardness were known as the parameters affecting the wear resistance of the composites experienced various pass numbers of the FSP. In comparison to the other composites, the 75Cu–25Fe-3 passes composite had the minimum wear resistance. Given Fig. 11, the weight loss of the 50Fe–50Cu-5 passes and 75Cu–25Fe-3 passes composites decreased by about 84% and 24%, respectively, compared to

the specimen processed without reinforcing powders at the sliding distance of 1000 m.

3.2.2.3 Wear Mechanisms Figure 12a and b show the low and high magnification FESEM images from the worn-out surface of the specimen processed without reinforcing powder. As can be seen, there was a high amount of the plastic deformation on the surface that is one of the main features of the adhesive wear. During the wear test, the aluminum pin and the steel disk are in contact with each other. Since there is a load between the pin and disk during the wear test, they are joined together and formed a solid state bond in the contact areas. Therefore, during the test, these contact areas are deformed and make the sliding more difficult leading to the increase in the friction coefficient and weight loss. In the adjacent of the deformed areas, imperfections like cavities and dislocations increase that promotes the formation of the micro cracks. These cracks then propagate and join to each other resulting in detachment of the surface layer and adhesive type of wear [35, 36].

The low and high magnification FESEM images from the worn-out surfaces of the composites are shown in Fig. 13. As can be seen in Fig. 13d and e, the 75Cu–25Fe-3 passes and 75Fe–25Cu-3 passes composites experienced plastic deformation which was again an evidence for the adhesive wear mechanism as explained before.

Figure 13f and j show the FESEM image from the worn-out surfaces of the 50Fe–50Cu-3 passes and 75Cu–25Fe-5 passes composites, respectively. In both composites, there were plate like debris and cracks which are evidences of the delamination wear [37–39]. In this mechanism, because of the wear process and the shear stress applied on the surface of the composite, the substance detaches from the worn surface and make the surface laminated. According to the delamination theory, shear stress of the wear action results in the plastic deformation and as a result, some cracks nucleate and grow in a bit depth of the surface. Eventually, these cracks can coalesce and cause the detachment of the substance. In fact, because of the severe plastic deformation caused by the FSP, dislocation density is relatively high in the subsurface regions before the wear test [12, 39, 40]. On the other hand, as a result of the plastic deformation, the dislocation density in the subsurface area increases during the wear process. Therefore, these dislocations can accumulate and form some pores beneath the area. Joining the pores during the wear process leads to the formation of the cracks and then, plate like debris are formed by the subsequent growth of these cracks [37, 41].

The backscattered electron FESEM images from the worn-out surfaces of the 75Fe–25Cu-5 passes and 50Fe–50Cu-5 passes composites are shown in Fig. 13k and l, respectively. As can be seen, there were some cracks on the worn-out surfaces indicating that the wear

Fig. 7 Grain structure of the base metal and the FSPed samples
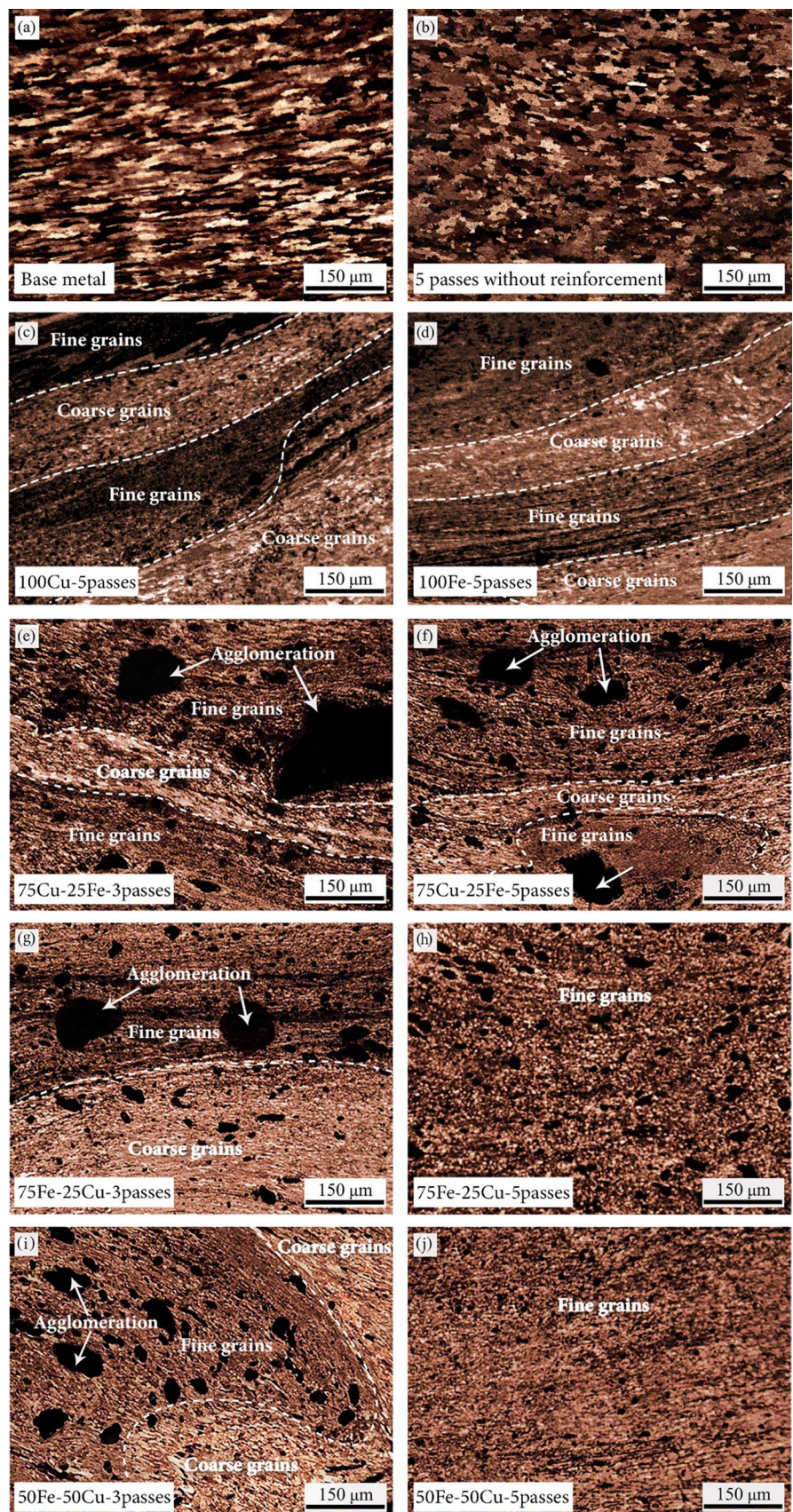
mechanism of these composites were delamination wear as explained above. According to the worn-out surfaces presented in Fig. 13, the wear mode was changed from the severe wear in the 75Cu–25Fe-3 passes and 75Fe–25Cu-3 passes composites to the mild wear in the 75Fe–25Cu-5 passes and 50Fe–50Cu-5 passes composites. This is attributed to the uniform distribution of the reinforcing particles. Regarding to Fig. 13k and l, some regions on the worn-out surfaces of the 75Fe–25Cu-5 passes and 50Fe–50Cu-5 passes composites contained a layer with a white contrast.

For more investigation, EDS analysis was performed on the points of A and B in Fig. 13k and l, respectively, and the

results are shown in Fig. 14. In both specimens, the layers contained a high weight percent of Cr and Fe atoms which there were in the composition of the disk used in the wear test. Consequently, mass transfer from the disk to the pins occurred during the wear test. Many previous researches [42, 43] confirmed that when mass transfer occurs between the sample and the counterpart during the wear test, a solid lubricated layer called *Mechanically Mixed Layer (MML)* is formed on the wear surface. In fact, this layer is formed by the atom interchanging between the pins and the disk during the wear test. Because of the strain hardening and the mechanical alloying, this layer has higher hardness compared to the pin that prevents it to be destroyed due to the
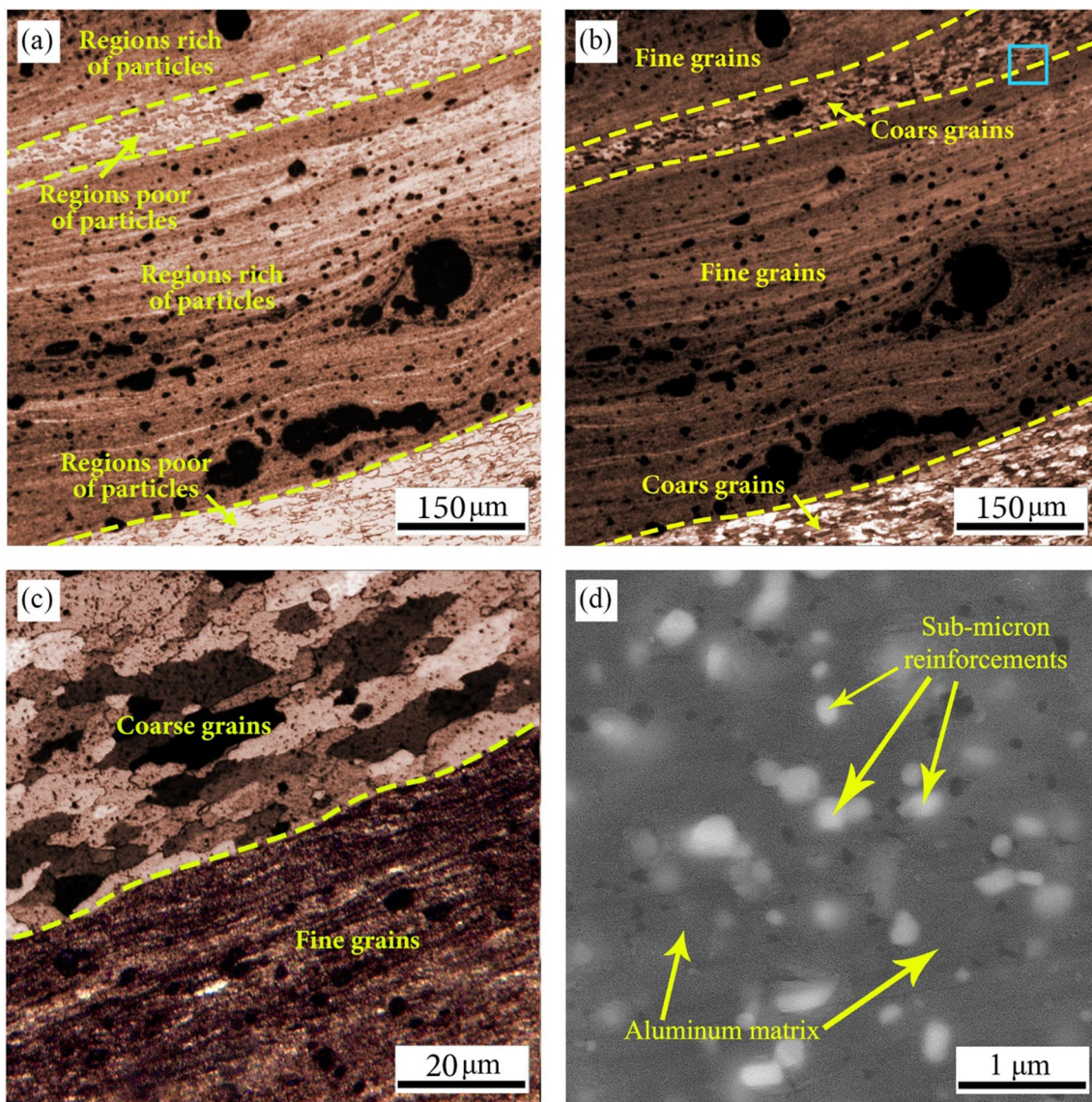

Fig. 8 Aluminum matrix microstructure of the 75Fe–25Cu-3 passes composite: **a** OM image before etching, **b** OM image after etching, **c** the magnified image from the rectangle in **b** including the bound-

ary between the coarse and fine grains, and **d** FESEM image from the broken and scattered particles in the fine grain regions
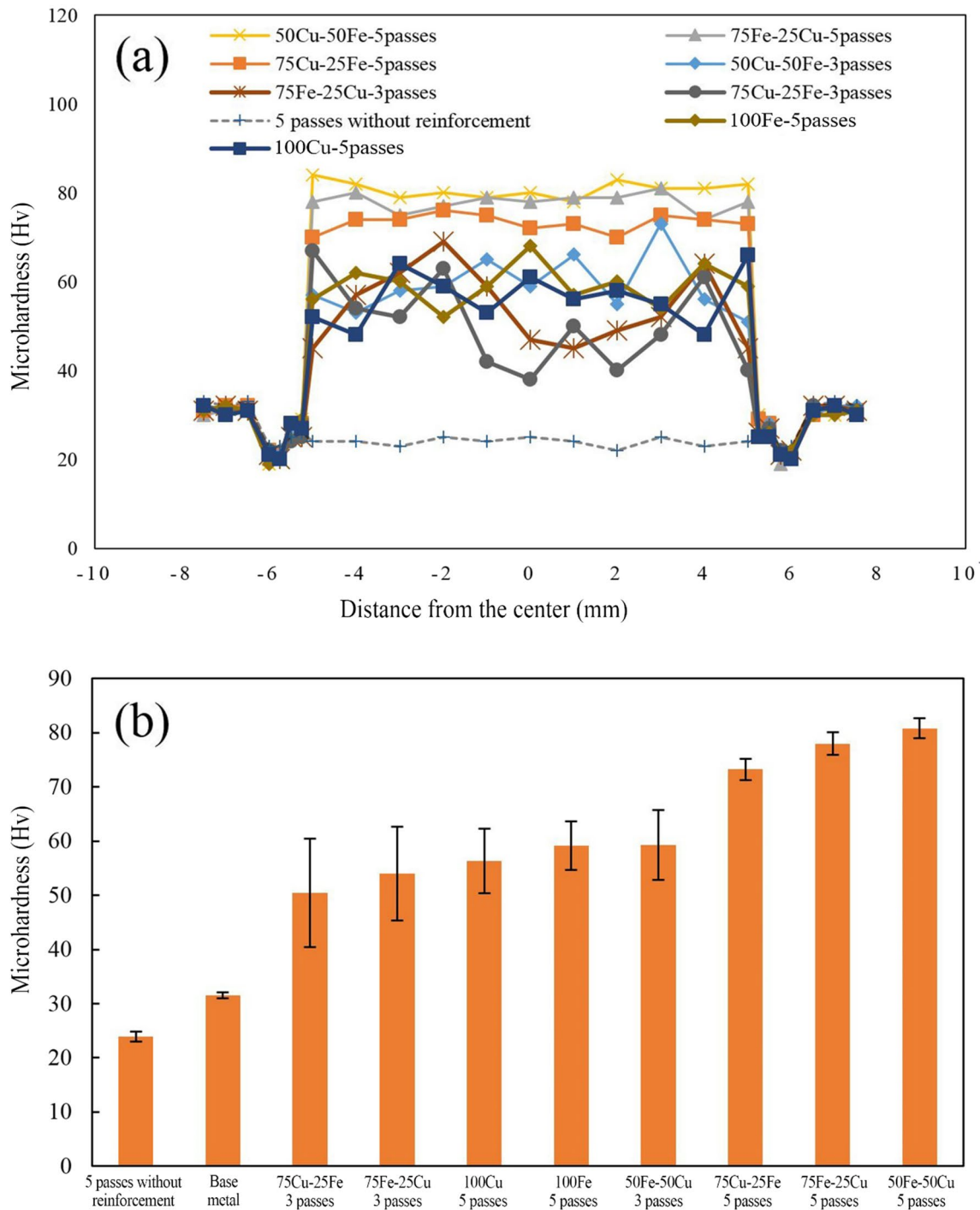
Fig. 9 **a** Microhardness profiles and **b** the average microhardness of the stir zones

imposed shear stress during the wear test. Moreover, the formation of this layer on the surface upsurges the thickness of the material which prevents the other adjacent areas to be involved in the wear process. Therefore, the MML improves the wear resistance of the composites [42, 43]. In the present

study, the MML layer was formed on the wear surface of the composites with the uniform fine grain structure and the homogeneous and consistent distribution of the reinforcing particles (i.e., composites with the powder weight ratios of 75Fe–25Cu and 50Fe–50Cu that were produced
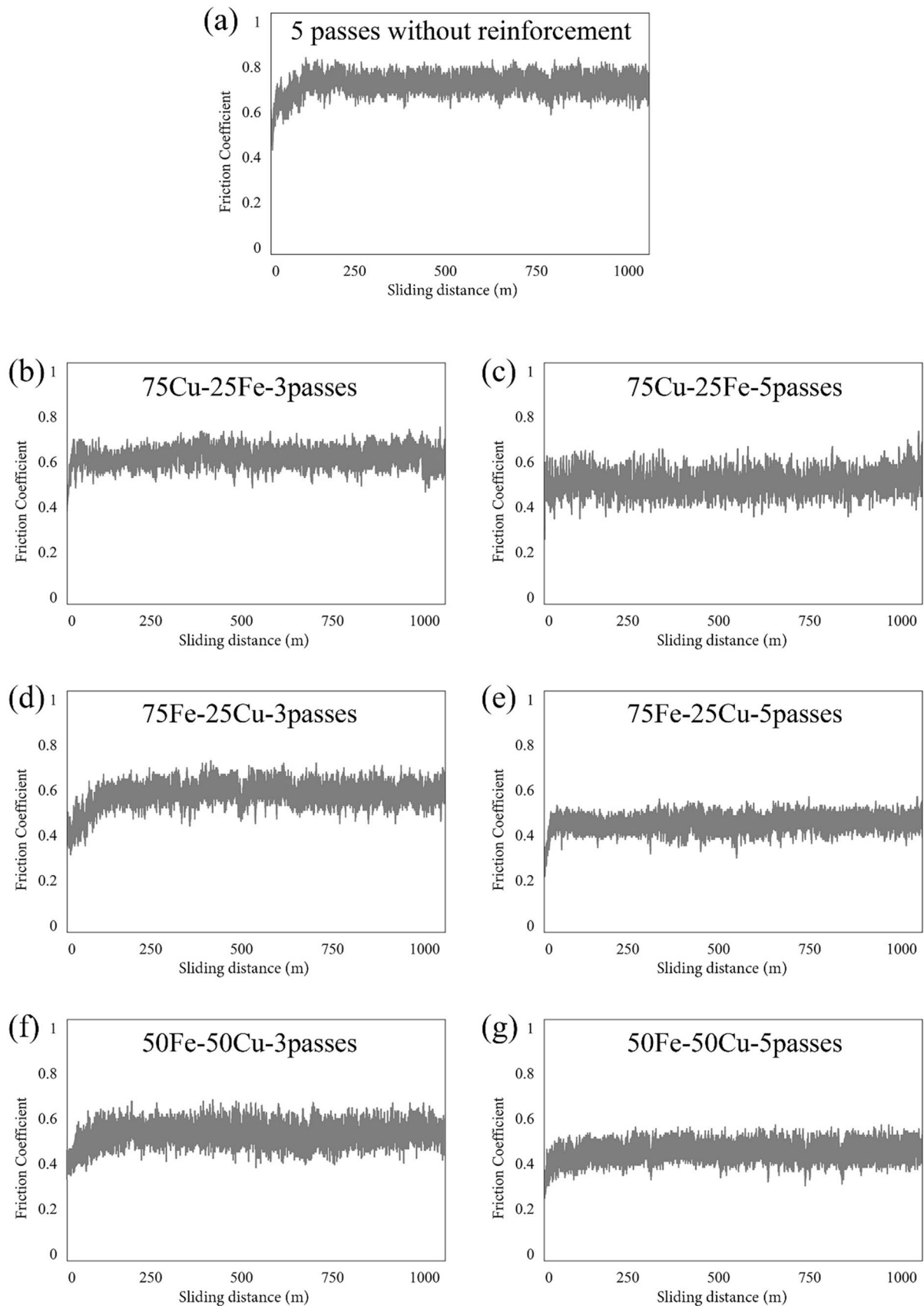
Fig. 10 Friction coefficient of the specimens versus the sliding distance

**Table 3** Average friction coefficient of the specimens

Sample	5 passes without reinforcement	75Cu–25Fe-3 passes	75Fe–25Cu-3 passes	50Fe–50Cu-3 passes	75Cu–25Fe-5 passes	75Fe–25Cu-5 passes	50Fe–50Cu-5 passes
Friction coefficient	0.74	0.61	0.59	0.56	0.52	0.46	0.44

Fig. 11 Weight loss of the specimens as a function of the wear sliding distance
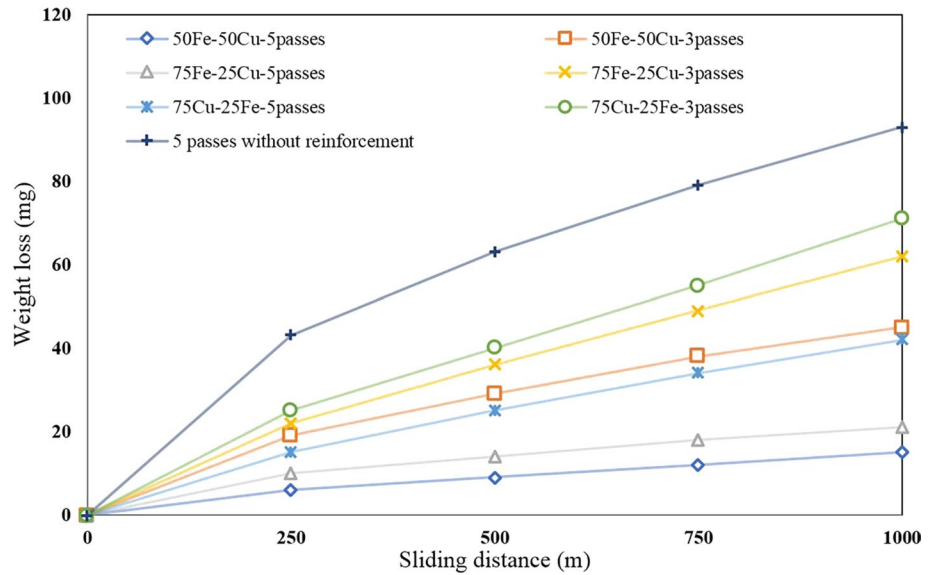
Fig. 12 **a** Low and **b** high magnification FESEM secondary electron images from the worn-out surface of the specimen processed at 5 passes without reinforcing particles
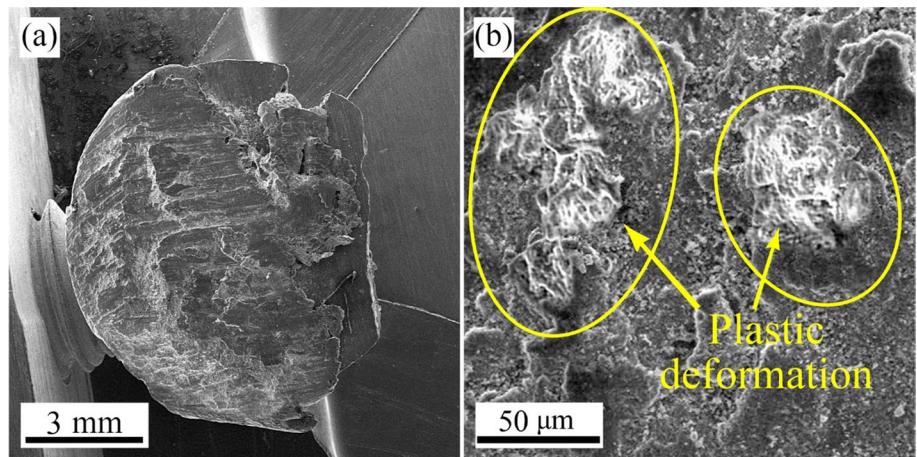
by 5 FSP pass number). Therefore, the low weight loss during the wear test in these composites may be attributed to the formation of the MML on the wear surface. Thus, it can be concluded that the homogeneous distribution of the reinforcing particles and the uniform grain structure of the composites play the main role in wear resistance [31, 44].

Fig. 13 **a**–**c** and **g**–**i** Low and **d**–**f** and **j**–**l** high magnification FESEM images from the worn-out surfaces of the composites. **a**–**g** and **j** are secondary electron and **h**, **i**, **k** and **l** are backscattered electron images
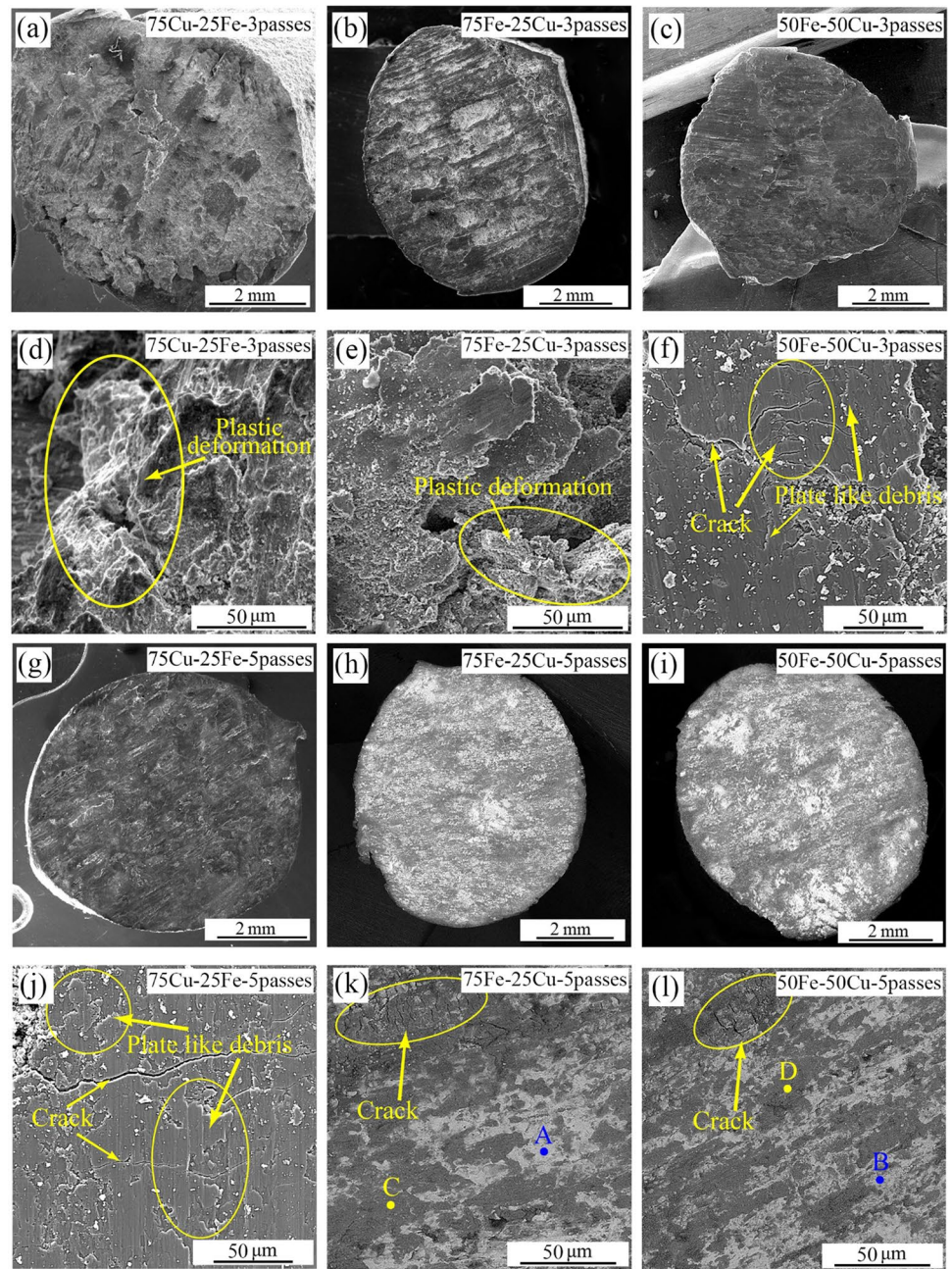
The size of wear debris in the 50Fe–50Cu-3 passes and 75Cu–25Fe-3 passes composites is shown in Fig. 15a and b, respectively. While the size of fine debris in the 75Cu–25Fe-3 passes specimen are in the range of sub-micron to ~ 1 μm, some large flakes with the size of ~ 5 μm are evident on the worn-out surface of the 50Fe–50Cu-3 passes composite. These large flakes are the result of delamination wear which is in agreement with the reports of the previous researches [45, 46].

Fig. 14 Chemical composition of the points **a** A and **b** B shown in the Fig. 13k and l, respectively

Composition (wt.%)			
Al	Fe	O	Cr
2	73	4	21

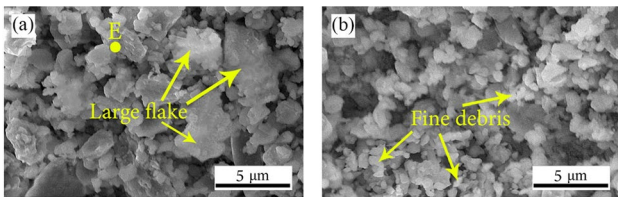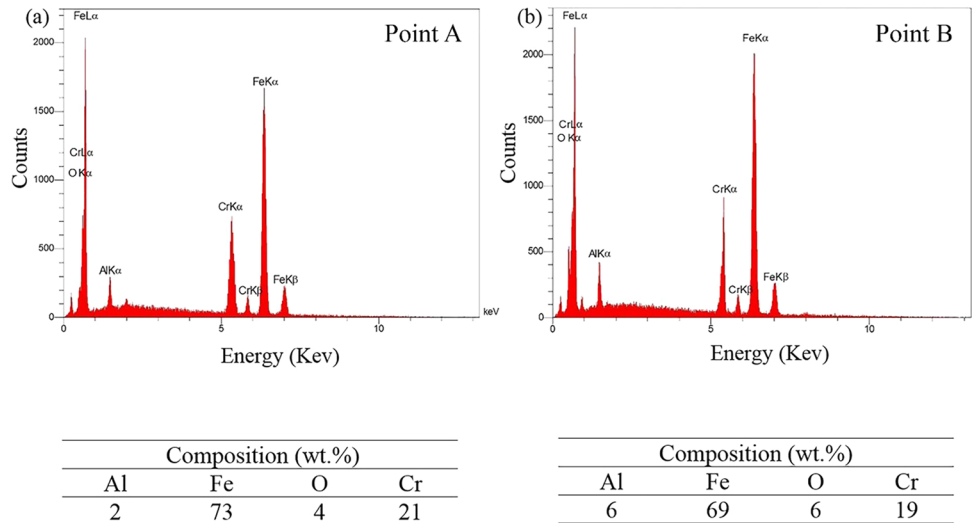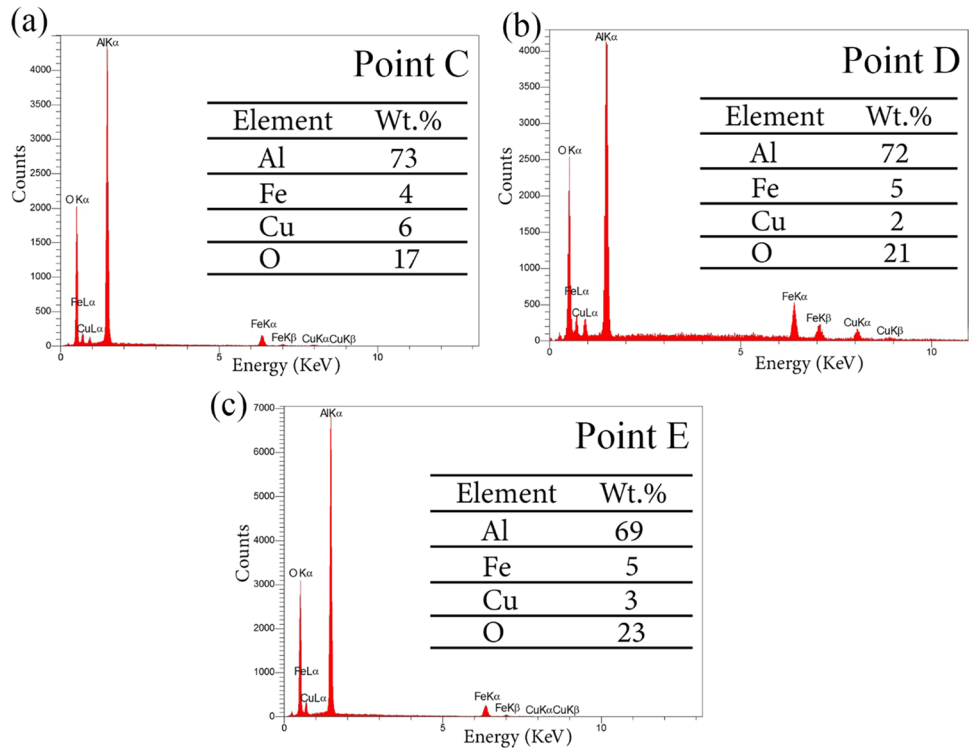| Composition (wt.%)			
Al	Fe	O	Cr
6	69	6	19

Fig. 15 Morphology of debris on the worn-out surfaces of **a** 50Fe–50Cu-3 passes and **b** 75Cu–25Fe-3 passes composites

EDS analysis was conducted at the regions C, D and E shown in Figs. 13 and 15 and the results are given in Fig. 16. According to the results, there is a considerable amount of oxygen element on the worn-out surfaces. Presence of the oxygen on the surfaces can be a sign of oxidation wear [47]. Indeed, along with the mentioned dominant wear mechanisms, the oxidation wear also happened in the composites during the wear test.

Fig. 16 Results of the EDS analysis conducted on the locations C, D and E shown in Figs. 13 and 15

Element	Wt.%
Al	73
Fe	4
Cu	6
O	17

Element	Wt.%
Al	72
Fe	5
Cu	2
O	21

Element	Wt.%
Al	69
Fe	5
Cu	3
O	23

4 Conclusion

Aluminum matrix hybrid composite was produced using micron-sized Fe and Cu particles via the friction stir processing. The effects of the weight fraction ratio of Fe and Cu powders in the composite and the FSP pass number (3 and 5 passes) were evaluated on the microstructural characteristics and wear behavior of the composite. The results are summarized as follows:

1. Due to the high temperature and interdiffusion of Al/Fe–Cu atoms, intermetallic compound layers of Al_2Cu, AlCu, Al_3Fe, and Al_5Fe_2 were in-situ formed at the interface of Al matrix and powders in the composite. These layers were subsequently shattered due to the stirring action of the FSP tool and dispersed in the Al matrix.
2. The non-homogeneous distribution of the micron-sized and sub-micron reinforcing particles in the composite led to the formation of the bi-modal grain structure (coarse and fine grain regions) in the aluminum matrix.
3. Fe/Cu powder weight ratio significantly affected the distribution of the reinforcing particles in the composite. In a constant FSP pass number, the best distribution of the reinforcements was related to the composites with the equal weight ratio of Fe and Cu powders due to the reduction of the intimate contact and bonding between the similar particles. Enhancement of the FSP pass numbers from 3 to 5 passes resulted in the consistency of the reinforcements distribution and grain structure. Consequently, the 50Fe–50Cu-5 passes composite showed the most homogeneous microstructure.
4. The microhardness of the composite with the most uniform microstructure (50Fe–50Cu-5 passes) increased ~3 times compared to the specimen processed at 5 passes without reinforcing powder.
5. By compositing, the average friction coefficient decreased up to ~40%. Additionally, the weight loss of the 50Fe–50Cu-5 passes composite decreased considerably (up to 84%) compared to the specimen processed without the reinforcing particles.
6. The wear mechanism was changed from the adhesive wear in the 75Cu–25Fe-3 passes and 75Fe–25Cu-3 passes composites to the delamination wear in the 50Fe–50Cu-5 passes composites. Uniform distribution of the reinforcing particles in the composite resulted in the formation of the mechanically mixed layer (MML).

Declarations

References

1. T. Arunkumar, V. Pavanan, V.A. Murugesan, V. Mohanavel, K. Ramachandaran, Met. Mater. Int. **28**, 145 (2022). https://doi.org/10.1007/s12540-021-01036-0
2. X. Yang, Z. Yan, P. Dong, B. Cheng, J. Zhang, T. Zhang, H. Zhang, W. Wang, Surf. Coat. Tech. **385**, 125438 (2020). https://doi.org/10.1016/j.surfcoat.2020.125438
3. M.A. Shaik, B.R. Golla, Wear **450–451**, 203260 (2020). https://doi.org/10.1016/j.wear.2020.203260
4. Y. Xie, X. Meng, Y. Huang, J. Li, J. Cao, Compos. Part B Eng. **177**, 107413 (2019). https://doi.org/10.1016/j.compositesb.2019.107413
5. R.S. Mishra, Z.Y. Ma, I. Charit, Mater. Sci. Eng. A **341**, 307 (2003). https://doi.org/10.1016/S0921-5093(02)00199-5
6. W.P. Bates, V. Patel, H. Rana, J. Andersson, J.D. Backer, M. Igestrand, L. Fratini, Met. Mater. Int. **29**, 215 (2023). https://doi.org/10.1007/s12540-022-01207-7
7. F.J. Humphreys, M. Hatherly, *Recrystallization and Related Annealing Phenomena*, 2nd edn. (Pergamon, Oxford, 2004)
8. V.S. Mann, O.P. Pandey, Wear **477**, 203801 (2021). https://doi.org/10.1016/j.wear.2021.203801
9. S.O. Akinwamide, O.J. Akinribide, P.A. Olubambi, J. Alloys Compd. **850**, 156586 (2021). https://doi.org/10.1016/j.jallcom.2020.156586
10. M.M. Khan, M. Nisar, Wear **488–489**, 204082 (2022). https://doi.org/10.1016/j.wear.2021.204082
11. X. Meng, Y. Huang, S. Liu, Y. Xie, J. Li, L. Zhou, Adv. Eng. Mater. **21**, 1800841 (2019). https://doi.org/10.1002/adem.201800841
12. G. Huang, W. Hou, J. Li, Y. Shen, Surf. Coat. Tech. **344**, 30 (2018). https://doi.org/10.1016/j.surfcoat.2018.03.005
13. P. Abhishek, E. Vimal, B.M. Abhishek, S.P. Chandra, H. Rajneesh, V.K. Satish, Mater. Today Commun. **24**, 101123 (2020). https://doi.org/10.1016/j.mtcomm.2020.101123
14. T. Thankachan, K.S. Prakash, V. Kavimani, Compos. Part B Eng. **174**, 107057 (2019). https://doi.org/10.1016/j.compositesb.2019.107057
15. B. Abnar, M. Kazeminezhad, A.H. Kokabi, J. Mater. Eng. Perform. **24**, 1086 (2015). https://doi.org/10.1007/s11665-014-1373-1
16. M.S. Khorrami, S. Samadi, Z. Janghorban, M. Movahedi, Mater. Sci. Eng. A **641**, 380 (2015). https://doi.org/10.1016/j.msea.2015.06.071
17. C.J. Hsu, P.W. Kao, N.J. Ho, Scr. Mater. **53**, 341 (2005). https://doi.org/10.1016/j.scriptamat.2005.04.006
18. E.R.I. Mahmoud, A.M.A. Al-qozaim, Arab. J. Sci. Eng. **41**, 1757 (2016). https://doi.org/10.1007/s13369-015-1889-1
19. T.B. Massalski, *Binary Alloy Phase Diagrams* (American Society for Metals, Ohio, 1986)
20. ASM Handbook Committee, *Alloy Phase Diagrams*, ASM Handbook, vol. 3 (ASM International, Materials Park, 1992)
21. M. Movahedi, A.H. Kokabi, S.M. Seyed Reihani, H. Najafi, S.A. Farzadfar, W.J. Cheng, C.J. Wang, Mater. Charact. **90**, 121 (2014). https://doi.org/10.1016/j.matchar.2014.01.023
22. R.D. Doherty, D.A. Hughes, F.J. Humphreys, J.J. Jonas, D.Juul Jensen, M.E. Kassner, W.E. King, T.R. McNelley, H.J. McQueen, A.D. Rollett, Mater. Sci. Eng. A **238**, 219 (1997). https://doi.org/10.1016/S0921-5093(97)00424-3

23. M. Azizieh, A.H. Kokabi, P. Abachi, Mater. Des. **32**, 2034 (2011). https://doi.org/10.1016/j.matdes.2010.11.055

24. C.J. Hsu, C.Y. Chang, P.W. Kao, , N.J. Ho, C.P. Chang, Acta Mater. **54**, 5241 (2006). https://doi.org/10.1016/j.actamat.2006.06.054

25. M. Eid, S. Kaytbay, A. El-Assal, O. Elkady, Met. Mater. Int. **28**, 2747 (2022). https://doi.org/10.1007/s12540-022-01177-w

26. M. Paidar, O.O. Ojo, H.R. Ezatpour, A. Heidarzadeh, Surf. Coat. Tech. **361**, 159 (2019). https://doi.org/10.1016/j.surfcoat.2019.01.043

27. B. Bhushan, *Modern Tribology Handbook* (CRC Press, Boca Raton, 2001)

28. E.R.I. Mahmoud, M. Takahashi, T. Shibayanagi, K. Ikeuchi, Wear **268**, 1111 (2010). https://doi.org/10.1016/j.wear.2010.01.005

29. J. Qiu, Z. Fu, B. Liu, J. Yan, D. Pan, W. Zhang, Met. Mater. Int. **25**, 1564 (2019). https://doi.org/10.1007/s12540-019-00279-2

30. U.P. Nayak, F. Mucklich, M.A. Guitar, Met. Mater. Int. **29**, 934 (2023). https://doi.org/10.1007/s12540-022-01276-8

31. M.A. Yaghoubi, N. Anjabin, H.S. Kim, Met. Mater. Int. (2023). https://doi.org/10.1007/s12540-023-01398-7

32. Mahesh, V. Koti, K.K. Singh, R.K. Singh, Wear **500–501**, 204368 (2022). https://doi.org/10.1016/j.wear.2022.204368

33. R. Hou, M. Wu, Q. Li, W. Li, D.L. Chen, D.Y. Li, Met. Mater. Int. **27**, 4911 (2021). https://doi.org/10.1007/s12540-020-00801-x

34. C. Qiao, J. Yu, S. Zhang, Z. Liu, J. Wang, Met. Mater. Int. **28**, 666 (2022). https://doi.org/10.1007/s12540-021-01138-9

35. L. Xia, B. Jia, J. Zeng, J. Xu, Mater. Charact. **60**, 363 (2009). https://doi.org/10.1016/j.matchar.2008.10.008

36. X. Jincheng, Y. Hui, X. Long, L. Xiaolong, Y. Hua, Mater. Des. **25**, 489 (2004). https://doi.org/10.1016/j.matdes.2004.01.011

37. A.A. Vereschaka, S.N. Grigoriev, Wear **378–379**, 43 (2017). https://doi.org/10.1016/j.wear.2017.01.101

38. F. Karpasand, A. Abbasi, M. Ardestani, Surf. Coat. Tech. **390**, 125680 (2020). https://doi.org/10.1016/j.surfcoat.2020.125680

39. H. Sarmadi, A.H. Kokabi, S.M. Seyed Reihani, Wear **340**, 1 (2013). https://doi.org/10.1016/j.wear.2013.04.023

40. A. Moharrami, A. Razaghian, M. Paidar, M. Slapakova, O.O. Ojo, R. Taghiabadi, Mater. Chem. Phys. **250**, 123066 (2020). https://doi.org/10.1016/j.matchemphys.2020.123066

41. T. Dixit, I. Singh, K.E. Prasad, Wear **420–421**, 207 (2019). https://doi.org/10.1016/j.wear.2018.10.021

42. M.R. Rosenberger, C.E. Schvezov, E. Forlerer, Wear **259**, 590 (2005). https://doi.org/10.1016/j.wear.2005.02.003

43. X.Y. Li, K.N. Tandon, Wear **225–229**, 640 (1999). https://doi.org/10.1016/S0043-1648(99)00021-6

44. M. Eftekhari, M. Movahedi, A.H. Kokabi, J. Mater. Eng. Perform. **26**, 3516 (2017). https://doi.org/10.1007/s11665-017-2752-1

45. P. Xiao, Y. Gao, F. Xu, C. Yang, Y. Li, Z. Liu, Q. Zheng, Tribol. Int. **128**, 130 (2018). https://doi.org/10.1016/j.triboint.2018.07.003

46. A. Meher, M.M. Mahapatra, P. Samal, P.R. Vundavilli, Met. Mater. Int. **27**, 3652 (2021). https://doi.org/10.1007/s12540-020-00746-1

47. R. Zheng, N. Li, Met. Mater. Int. **27**, 1103 (2021). https://doi.org/10.1007/s12540-019-00489-8